

Cardiac-derived TGF- β 1 confers resistance to diet-induced obesity through the regulation of adipocyte size and function



Jacob Z. Longenecker¹, Jennifer M. Petrosino¹, Colton R. Martens¹, Scott A. Hinger¹, Charlotte J. Royer¹, Lisa E. Dorn¹, Daniel A. Branch¹, Joan Serrano², Kristin I. Stanford¹, George A. Kyriazis², Kedryn K. Baskin¹, Federica Accornero^{1,*}

ABSTRACT

Regulation of organismal homeostasis in response to nutrient availability is a vital physiological process that involves inter-organ communication. Understanding the mechanisms controlling systemic cross-talk for the maintenance of metabolic health is critical to counteract diet-induced obesity. Here, we show that cardiac-derived transforming growth factor beta 1 (TGF- β 1) protects against weight gain and glucose intolerance in mice subjected to high-fat diet. Secretion of TGF- β 1 by cardiomyocytes correlates with the bioavailability of this factor in circulation. TGF- β 1 prevents adipose tissue inflammation independent of body mass and glucose metabolism phenotypes, indicating protection from adipocyte dysfunction-driven immune cell recruitment. TGF- β 1 alters the gene expression programs in white adipocytes, favoring their fatty acid oxidation and consequently increasing their mitochondrial oxygen consumption rates. Ultimately, subcutaneous and visceral white adipose tissue from cardiac-specific TGF- β 1 transgenic mice fail to undergo cellular hypertrophy, leading to reduced overall adiposity during high-fat feeding. Thus, TGF- β 1 is a critical mediator of heart-fat communication for the regulation of systemic metabolism.

© 2021 The Authors. Published by Elsevier GmbH. This is an open access article under the CC BY-NC-ND license (<http://creativecommons.org/licenses/by-nc-nd/4.0/>).

Keywords TGFbeta; Heart; Mitochondria

1. INTRODUCTION

The current Western lifestyle plagues the human population worldwide with metabolic disorders driven by excess caloric intake. Diet-induced obesity has become a clinical concern of epic proportions [1]. Although the behavior of white adipose tissue is central to the onset of obesity, circulating factors can affect adipocyte function, allowing distal organs to play a critical role in the regulation of adiposity [2]. Indeed, in higher organisms, complex interplay between organ systems coordinates responses to nutrient availability [3,4]. Elucidating the mechanisms underlying inter-organ cross-talk for the maintenance of systemic metabolic health is essential for unravelling the vital homeostatic processes that govern adaptation to dietary challenges.

While several organs such as the brain, liver, pancreas and skeletal muscle have been extensively studied for their ability to influence adipocyte biology [4], the function of the heart in the regulation of adiposity is a less studied subject. The heart has long been recognized as an endocrine organ capable of secreting pleiotropic circulating factors [5,6]. Conversely, the heart is also able to sense adipokine levels and respond to them [7]. However, a paradox exists where greater adiposity increases the risk of cardiac dysfunction while low

body fat mass percentage correlates with worse heart failure outcomes [8]. Unintentional weight loss is a poor prognosis parameter that is linked to reduced survival in heart failure patients [9]. A consensus on the identity of the key mediators of this paradoxical heart-adipose tissue axis is still missing.

Transforming growth factor beta 1 (TGF- β 1) is locally activated in response to organ injuries [10]. Increased TGF- β 1 bioavailability is typically considered to be a pathological marker of tissue remodeling that drives fibrosis as part of the wound healing process [11,12]. In the heart, TGF- β 1 is sufficient to drive dysfunction and single cell analysis revealed ubiquitous expression of its receptors [13–15]. TGF- β 1 is activated in response to cardiac injuries such as pressure overload-induced remodeling as well as in ischemic heart disease [13,14]. However, the impact of this growth factor as a systemic messenger for the heart has not been recognized previously. Here, we identified TGF- β 1 as a critical mediator of heart communication to white fat depots that control adipocyte function and systemic metabolic responses to high-fat diet. By adopting a mouse model that mimics the cardiac activation of TGF- β 1 that occurs in the case of animal and human heart injuries, we show how the heart secretes TGF- β 1 into the bloodstream to induce the systemic effects that underlie the heart–adipose tissue cross talk.

¹Department of Physiology and Cell Biology, Dorothy M. Davis Heart and Lung Research Institute, The Ohio State University, Columbus, OH, USA ²Department of Biological Chemistry and Pharmacology, Dorothy M. Davis Heart and Lung Research Institute, The Ohio State University, Columbus, OH, USA

*Corresponding author. E-mail: federica.accornero@osumc.edu (F. Accornero).

Received July 21, 2021 • Revision received September 20, 2021 • Accepted September 21, 2021 • Available online 25 September 2021

<https://doi.org/10.1016/j.molmet.2021.101343>

2. RESULTS

2.1. TGF- β 1 activated by the heart is secreted into the bloodstream with mild impact on the cardiac structure and function following high-fat diet

TGF- β 1 is activated under cardiac stress conditions [13]. To elucidate the systemic metabolic impact of cardiac-derived TGF- β 1, we adopted a mouse model that mimics the expression level of bioavailable TGF- β 1 in the heart following injuries and challenged these mice to caloric excess by high-fat diet (Figure 1A). This

cardiomyocyte-specific model expresses a mutant form of TGF- β 1 that cannot bind the latency complex and therefore its bioavailability is not inhibited [13]. The 6-week high-fat diet timeframe was chosen to avoid cardiac complications derived from long-term TGF- β 1 activation, which would confound our results. Independent of the diet, we validated the increase in bioavailable TGF- β 1 in the hearts of our transgenic mice expressing mutant TGF- β 1 (TGF) versus littermate controls expressing wild-type TGF- β 1 level and form (WT) (Figure 1B). On the other hand, the total TGF- β 1 levels were not significantly impacted above physiological levels in neither the

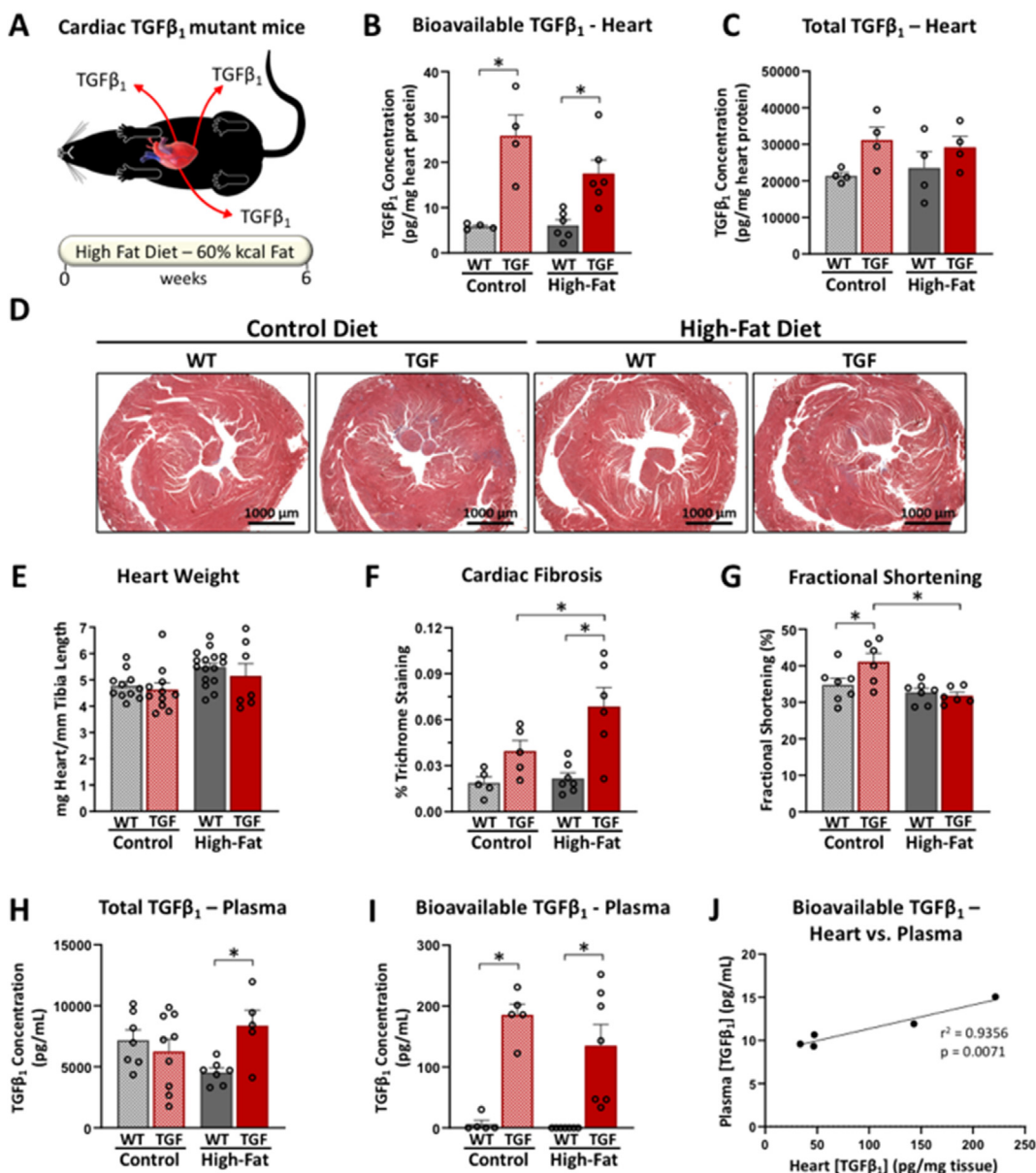


Figure 1: Cardiac phenotype of heart-specific TGF- β 1 mutant mice subjected to high-fat diet. (A) Schematic detailing cardiac-specific overexpression of TGF- β 1 in TGF mutant mice and the high-fat diet regimen used to induce obesity. (B, C) ELISA showing the amount of bioavailable (active) and total (latent plus active) TGF- β 1 locally in the heart under control or high-fat diet in WT or TGF mice. (D) Trichrome staining on cardiac sections, (E) heart mass normalized to tibia length, (F) quantification of % cardiac fibrosis from trichrome-stained sections, and (G) echocardiographic analysis of fractional shortening from the indicated genotypes and conditions. (H, I) ELISA showing the amount of total (latent plus active) and bioavailable (active) TGF- β 1 locally in the plasma under control or high-fat diet in WT or TGF mice. (J) Correlation between heart and plasma level of bioavailable TGF- β 1 in TGF mice under high-fat diet. Statistics were calculated using a two-way ANOVA, where * indicates $p < 0.05$. Data are presented as the mean \pm SEM. Groups sizes are listed in the order of control diet WT, control diet TGF, high-fat diet WT, and high-fat diet TGF: (B) $n = 4, 4, 6, 5$; (C) $n = 4, 4, 4, 4$; (E) $n = 11, 11, 16, 7$; (F) $n = 5, 5, 7, 6$; (G) $n = 7, 6, 7, 6$; (H) $n = 7, 9, 7, 5$; and (I) $n = 5, 5, 7, 7$.

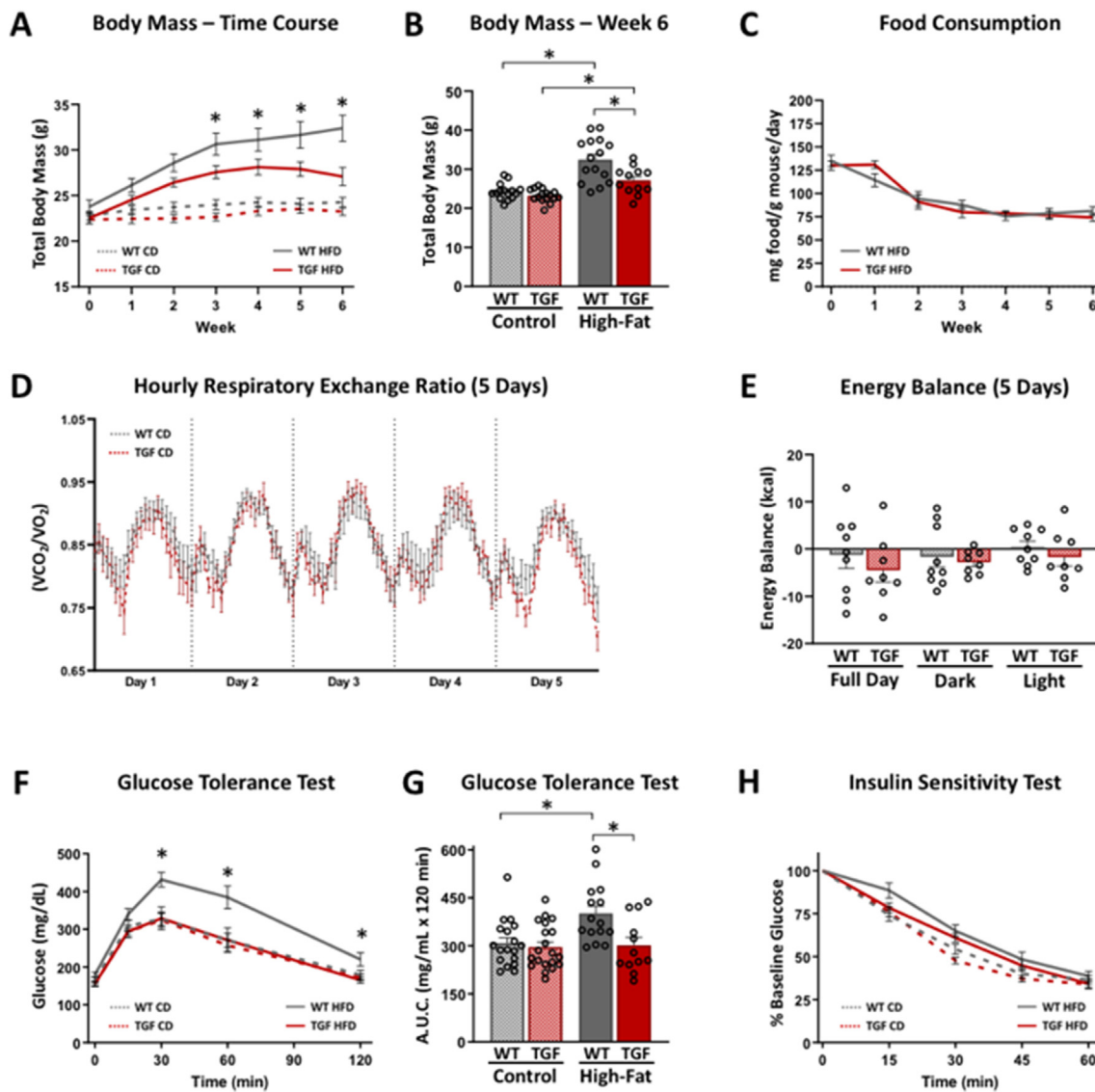


Figure 2: Whole-body metabolism is affected by cardiac-derived TGF- β 1 with high-fat diet. (A, B) Body mass of WT and TGF mice under control or high-fat diet at the indicated time points. CD = control diet; HFD = high-fat diet. (C) Weekly food consumption over the course of 6 weeks of high-fat feeding in WT and TGF mice. (D) Average hourly respiratory exchange ratio (RER), and (E) and average energy balance (energy intake–energy expenditure) over 5 days of control diet consumption of WT and TGF mice in metabolic cages. (F, G) Glucose tolerance test (A.U.C. = area under the curve in (G)), and (H) insulin sensitivity test in WT and TGF mice following 6 weeks of control or high-fat diet. Statistics were calculated either using a two-way ANOVA when more than two groups were compared (panels A–C and F–H) or the Student's t-test when two groups were compared (panels C–E), where * indicates $p < 0.05$. Data are presented as the mean \pm SEM. Groups sizes are listed in the order of CD WT, CD TGF, HFD WT, and HFD TGF: (A, B) $n = 15, 16, 15, 12$; (C) $n = 6, 4$ (HFD only); (D, E) $n = 9, 8$ (CD only); (F, G) $n = 18, 20, 15, 12$; and (H) $n = 19, 18, 15, 12$.

control group nor the high-fat diet group (Figure 1C). Importantly, the levels of bioavailable TGF- β 1 in TGF mice do not surpass the degree of TGF- β 1 activation observed when the heart is injured by 4 weeks of transverse aortic constriction (TAC) to induce pressure overload-driven heart failure (Figure S1A). Cardiac structure and size were unaffected in TGF mice under both control and high-fat-diet conditions (Figure 1D, E; Table S1). However, a mild induction of cardiac fibrosis was significantly exacerbated by the high-fat diet (Figure 1F). Importantly, no cardiac dysfunction was observed in our model and the high-fat diet did not induce any genotype-dependent effects on fractional shortening, a measure of cardiac contractility (Figure 1G). Indeed, while fractional shortening was even increased in TGF mice on control diet, this phenomenon was not detected during the high-

fat diet regimen (Figure 1G and Table S1). Analysis of the cardiomyocyte area and hypertrophic gene expression did not reveal significant genotype-dependent changes, although a trend toward an increase in atrial natriuretic peptides (Nppa and Nppb) was observed in TGF mice (Figure S1B–E). The total circulating TGF- β 1 levels were similar in WT and TGF mice on control diet, but higher levels were observed in TGF mice on high-fat diet (Figure 1H). This is likely due to a trend towards lower circulating TGF- β 1 levels in WT on high-fat diet, which was prevented in TGF- β 1 mutant mice. Strikingly, the activation of TGF- β 1 in the heart was sufficient to increase the circulating content of bioavailable TGF- β 1 (Figure 1I), and a strong correlation between cardiac and circulating level of active TGF- β 1 was noted in TGF mice under high-fat diet (Figure 1J).

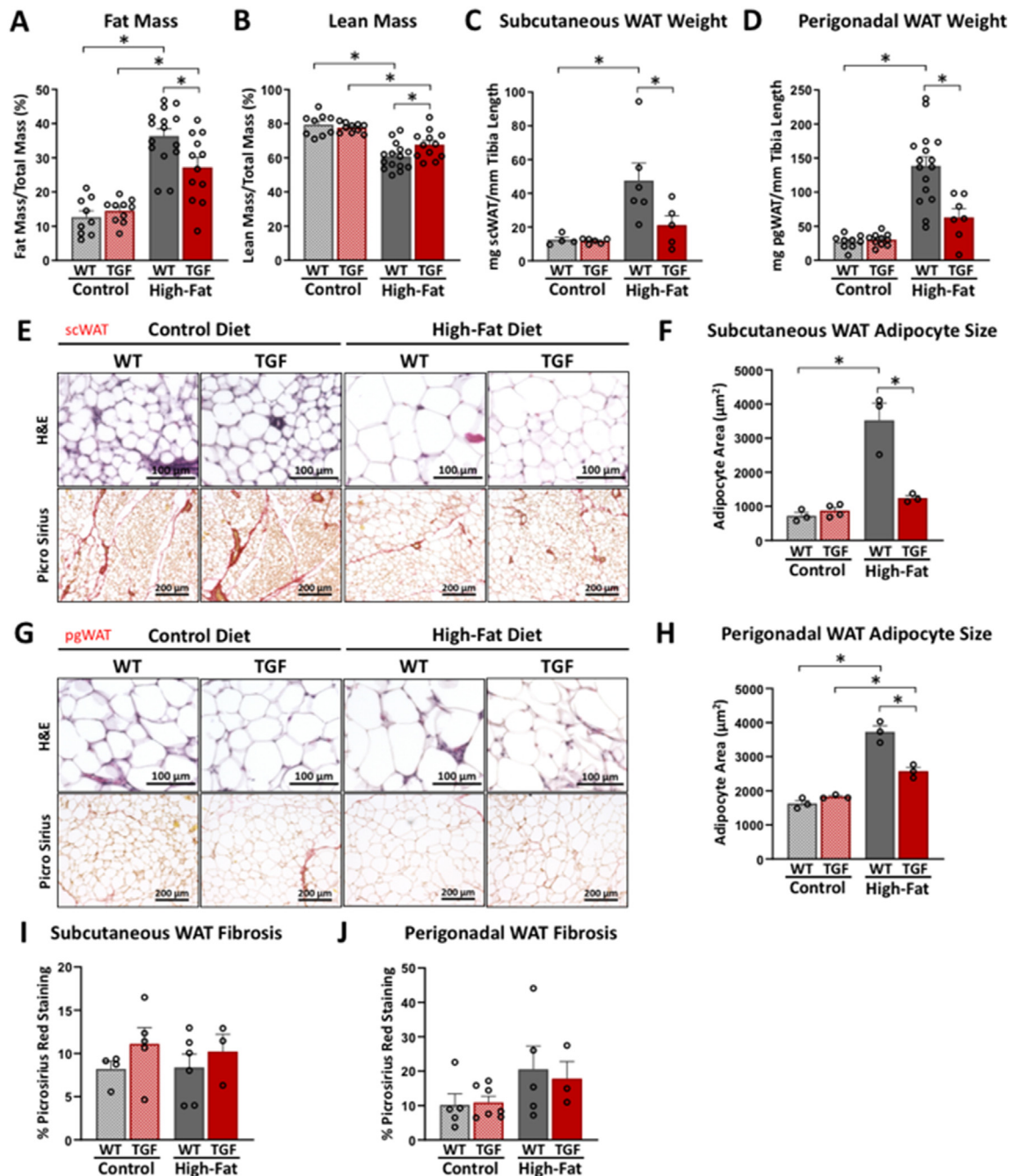


Figure 3: Cardiac-derived TGF- β 1 protects from diet-induced adipose tissue expansion. (A, B) EchoMRI body composition analysis of fat and lean mass from WT and TGF mice after 6 weeks of control (CD) or high-fat diet (HFD). (C, D) Subcutaneous and perigonadal white adipose tissue (scWAT and pgWAT, respectively) normalized to tibia length from WT and TGF mice after 6 weeks of control or high-fat diet. (E–J) Histological assessment of adipocyte size using H&E staining (top E and G panels; quantified in F and H), and adipose tissue fibrosis using Picro-Sirius red staining (bottom E and G panels; quantified in I and J) in the indicated fat depots and genotypes after 6 weeks of control or high-fat diet. Statistics were calculated using a two-way ANOVA, where * indicates $p < 0.05$. Data are presented as the mean \pm SEM. Groups sizes are listed in the order of CD WT, CD TGF, HFD WT, and HFD TGF: (A, B) $n = 9, 10, 15, 12$; (C) $n = 4, 6, 6, 5$; (D) $n = 9, 10, 16, 7$; (F) $n = 3, 4, 3, 3$; (H) $n = 3, 3, 3, 3$; (I) $n = 4, 5, 6, 3$; and (J) $n = 5, 7, 5, 3$.

2.2. Cardiac-derived TGF- β 1 protects against diet-induced body mass gain and glucose intolerance

Considering the observed correlation between cardiac and circulating TGF- β 1 bioavailability, we tested whether systemic responses were affected in our cardiac-specific transgenic mice. Body mass was monitored weekly and reduced weight gain was highlighted in TGF mice starting from 3 weeks following high-fat diet (Figure 2A). Overall,

while both genotypes responded to the diet challenge, the high-fat-diet-induced body mass increase was significantly blunted in TGF mice at the terminal time point (Figure 2B). This protection from body mass gain was independent of food consumption under high-fat diet (Figure 2C) and could not be explained by baseline alterations in fuel utilization or energy balance (Figure 2D, E). Interestingly, the glucose intolerance that is typically induced by high-fat-diet feeding was

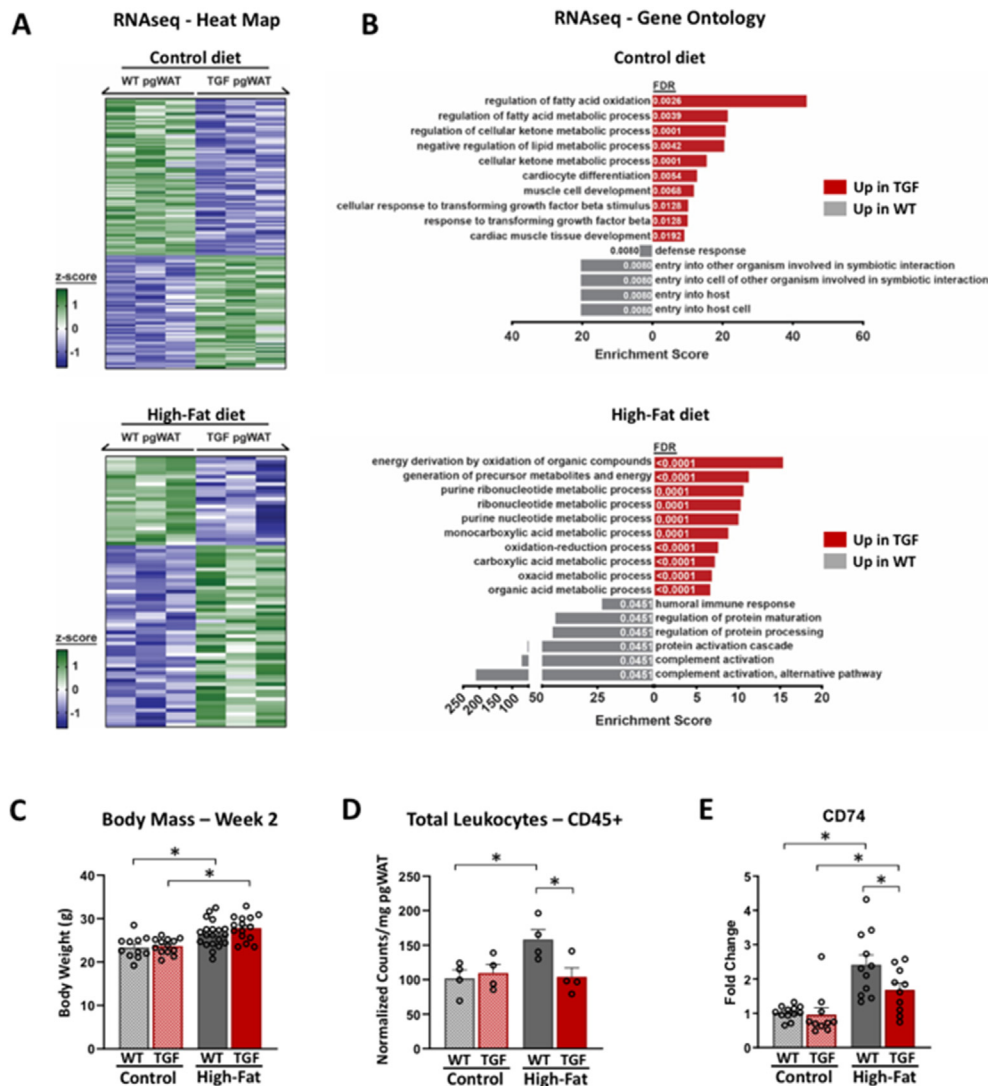


Figure 4: Cardiac-derived TGF- β 1 alters gene expression programs and inflammation in white adipose tissue. (A) Heat map generated using differentially expressed genes from RNA sequencing of perigonadal white adipose tissue (pgWAT) from WT and TGF mice under control and high-fat diet. (B) Gene ontology analysis comparing RNA sequencing of TGF and WT pgWAT under control and high-fat diet. (C) Body mass of WT and TGF mice following 2 weeks of control or high-fat diet. (D) Flow cytometry for CD45-positive cells (CD45+) in pgWAT from the indicated genotypes following 2 weeks of control or high-fat diet. (E) qPCR for CD74 normalized to *Ppia* housekeeping gene from pgWAT from the indicated genotypes following 2 weeks of control or high-fat diet. Statistics were calculated using a two-way ANOVA, where * indicates $p < 0.05$. Data are presented as the mean \pm SEM. Group sizes are listed in the order of CD WT, CD TGF, HFD WT, and HFD TGF: (A, B) $n = 3, 3$; (C) $n = 11, 13, 20, 15$; (D) $n = 4, 4, 4, 4$; and (E) $n = 12, 10, 11, 10$.

prevented in TGF mice (Figure 2F, G) independently from insulin sensitivity (Figure 2H).

2.3. Cardiac-derived TGF- β 1 affects the response of white adipose tissue to high-fat feeding

Since increased adiposity is a key determinant of body mass changes and obesity onset, we measured the body composition of our TGF mutant and control mice. Although fat mass increased significantly in mice fed high-fat diet, TGF mice gained significantly less fat (Figure 3A), and lost significantly less lean mass compared with that observed in control mice (Figure 3B). Subcutaneous and perigonadal visceral white adipose tissues (scWAT and pgWAT, respectively) are key contributors to body adiposity. Therefore, we weighed these fat depots and observed a significant reduction in fat mass in both depots in high-fat fed TGF mice (Figure 3C, D). Microscopic analysis of white

adipose tissue revealed smaller adipocytes in both subcutaneous and perigonadal depots (Figure 3E–H) in TGF mice subjected to high-fat diet, while fibrosis was unaffected (Figure 3E and G – bottom panels; Figures 3I, J). While white adipose tissue mass and metabolism play a critical role in the pathophysiological effects of obesity, other organs such as brown adipose tissue and liver play important roles in the systemic control of metabolism. Brown adipose tissue (BAT) from wild-type mice subjected to high-fat diet weighed more, and this increase was blunted in TGF animals (Figure S2A). However, the diet-induced increase in BAT lipid area or triglyceride content was not affected by our genotypes, and fibrosis was not impacted under any condition (Figures S2B–S1E). Interestingly, while the liver mass was unaffected, the triglyceride content increased with high-fat diet in control animals but not in TGF mice, and no induction of fibrosis was observed in the liver (Figures S2F–S1I).

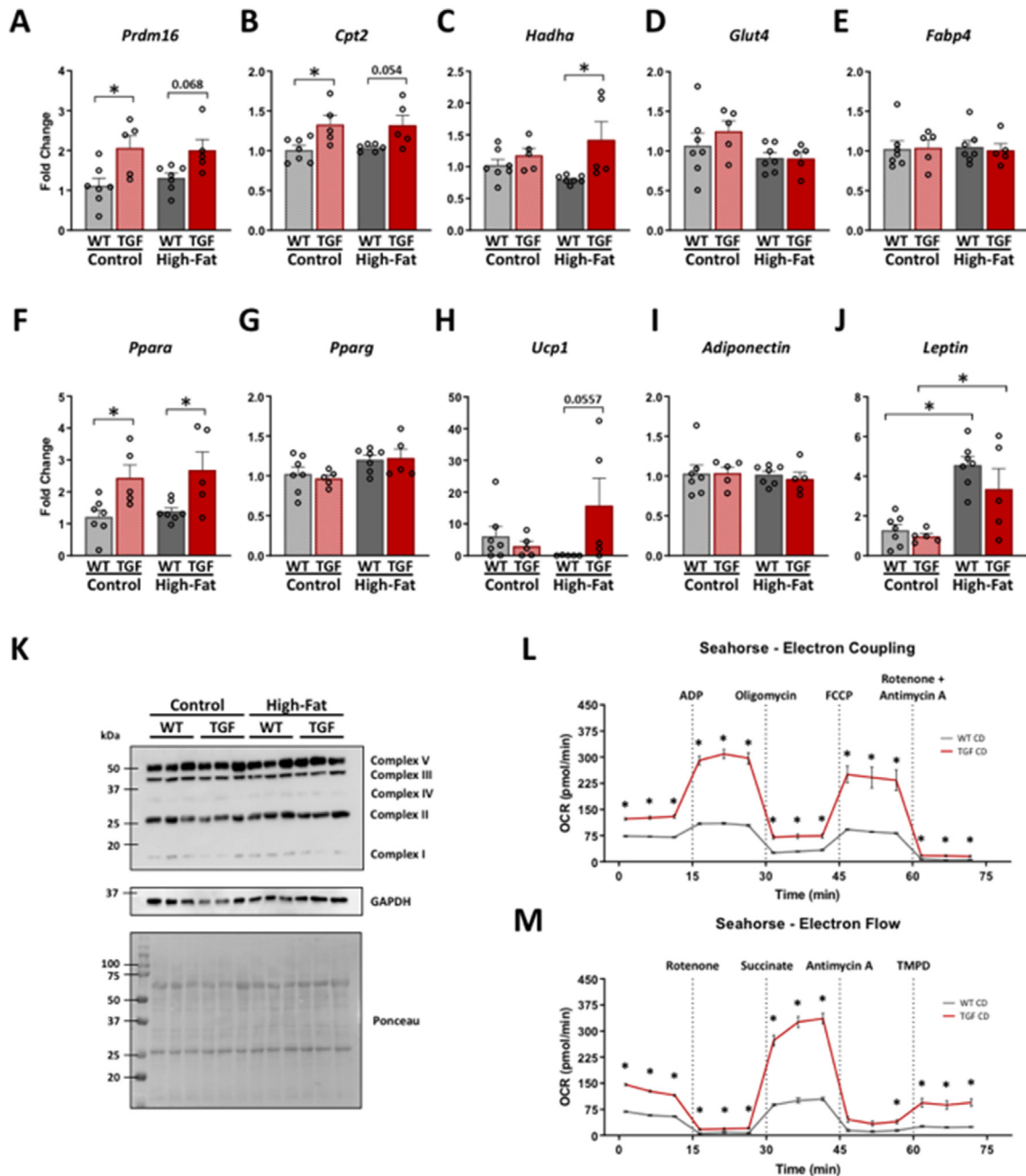


Figure 5: Cardiac-derived TGF- β 1 enhances adipocyte thermogenic gene expression and mitochondrial function. (A–J) qPCR for the indicated genes normalized to *Ppia* housekeeping gene from perigonadal white adipose tissue (pgWAT) of WT and TGF mice following 2 weeks of control (CD) or high-fat diet (HFD). (K) Western blot for OXPHOS complexes and GAPDH performed on protein extracts from pgWAT of WT and TGF mice following 2 weeks of control or high-fat diet; Ponceau red staining is shown as a loading control. (L, M) Seahorse electron coupling and flow assays on mitochondria isolated from pgWAT of WT and TGF mice under control diet; mitochondria were treated with the indicated electron transport chain chemical inhibitors and activators to highlight the OXPHOS complex function (ADP = adenosine diphosphate, FCCP = trifluoromethoxy carbonyl cyanide phenylhydrazine, TMPD = tetramethyl-p-phenylenediamine). Statistics were calculated using a two-way ANOVA (A–J) and the Student's t-test (L–M), where * indicates $p < 0.05$. Data are presented as the mean \pm SEM. Group sizes are listed in order of CD WT, CD TGF, HFD WT, and HFD TGF: (A, C–G, I–J) $n = 7, 5, 7, 5$; (B) $n = 7, 5, 6, 5$; (H) $n = 7, 5, 5, 5$; (K) $n = 3, 3, 3, 3$; and (L, M) $n = 8, 9$.

2.4. Regulation of adipocyte gene programs in cardiac-specific TGF- β 1 mutant mice

TGF- β 1 signaling alters gene expression through regulation of transcription [16]. To elucidate the mechanisms responsible for altered response to high-fat diet observed in TGF- β 1 mutant mice, we performed unbiased RNA expression analysis in pgWAT. This depot was

chosen as visceral white adipose depot is most critical for metabolic dysfunction in response to diet challenges [17,18]. This analysis revealed a profound impact of TGF- β 1 on the transcriptome of pgWAT under both control and high-fat diet conditions (Figure 4A, Table S2 and Table S3). In particular, we found 151 differentially expressed genes (65 up, 86 down) when we compared TGF versus WT pgWAT

under control diet, while 73 genes were regulated (49 up, 24 down) on high-fat diet (Table S2 and Table S3). Gene ontology analysis of differentially regulated transcripts highlighted downregulation of inflammation regulators in TGF mice as well as induction of fatty acid oxidation and transdifferentiation programming (Figure 4B). Considering the known deleterious effects of inflammation in obesity, we first assessed the impact of TGF- β 1 on immune cell infiltration following 2 weeks of high-fat diet. This time point was chosen to be in a situation of metabolic stress that precedes major genotype-dependent phenotypic changes that would confound the results (Figures 4C and S3A–S3D). Analysis of the total leukocytes in pgWAT revealed protection of TGF mice against high-fat-diet-induced inflammation (Figure 4D). This result was confirmed molecularly with reduced induction of the immune cell marker CD74 in TGF mice subjected to high-fat diet (Figure 4E), and the same trend was observed for lymphoid and myeloid lineages (Figures S3E and S3F). Importantly, abrogation of inflammatory infiltration preceded the changes in the body mass, glucose tolerance or adipose tissue mass (Figures 4C and S3A–S3D), and the 2-week high-fat diet regimen was adequate to determine some degree of TGF- β 1 canonical signaling activity while ERK1/2 was the dominant non-canonical activated pathway (Figure S4A–J). While the role of TGF- β 1 on inflammation was an important finding highlighted by our sequencing experiment and gene ontology analysis, we also observed significant induction of genes involved in cell metabolism and differentiation (Figure 4B). Changes in cell differentiation could not only explain the alteration in adipocyte inflammatory phenotypes but also further refine the mechanism underlying the observed protection from diet-induced obesity in TGF- β 1 mutant mice. Muscle and brown adipose tissue originate from the same progenitor cell, and mitochondrial function is a key feature for differentiating between brown and white adipose tissue [19]; therefore, we reasoned that the gene ontology definition of muscle differentiation could indicate a mitochondrial phenotype of pgWAT from TGF mice. Indeed, we observed the induction of *Prdm16* (Figure 5A). *Prdm16* can regulate the mitochondrial function in white adipose tissue [20]. Indeed, pgWAT from TGF- β 1 mutant mice displayed increased expression of the beta-oxidation regulators *Cpt2* and *Hadha* (Figure 5B, C), while *Glut4* (glucose uptake) and *Fabp4* (fatty acid transport) were unaffected (Figure 5D, E). Interestingly, *Ppar α* , and not *Ppar γ* , was specifically induced by TGF- β 1, and only a trend toward *Ucp1* induction was observed in high-fat-fed TGF mice (Figure 5F–H). In addition, no genotype-dependent differences were observed in the expression of adiponectin or leptin (Figure 5I, J). The consequence of the observed gene program changes was characterized by the analysis of mitochondrial content and activity, a distinguishing feature between BAT and WAT. While mitochondrial content was unchanged (Figure 5K), basal respiration was increased in mitochondria from TGF pgWAT and the enhanced mitochondrial function throughout all electron chain complexes were also significant, quantified using complementary electron coupling and electron flow assays (Figure 5L and 5M). Altogether, cardiac-derived TGF- β 1 alters the mitochondrial function of white adipocytes and prevents their inflammation and growth, providing overall protection from obesity onset under caloric excess.

3. DISCUSSION

The transforming growth factor (TGF) superfamily comprises several protein isoforms, of which TGF- β 1 is one of the best studied. Despite the extensive investigation that focused on this growth factor, its pleiotropic nature and context-dependent activity contribute to a great complexity of regulation and effects that has obfuscated some of its

fundamental biological roles in higher organisms. Our study highlighted TGF- β 1 as a critical mediator of heart-driven regulation of adipose tissue plasticity. While our work focused on the heart as a source of TGF- β 1, it is possible that such a mechanism could be valid in other organs where TGF- β 1 is induced in response to injury. Indeed, chronic diseases such as congestive heart failure, cancer, or chronic obstructive pulmonary fibrosis are all characterized by dysregulated TGF- β 1 signaling as well as adipose tissue wasting and cachexia [21–24]. While injury-induced activation of TGF- β 1 has been locally studied in each specific targeted organ, how this induction could facilitate inter-organ communication is not yet fully clear. Our data support a mechanism by which the local bioavailability of TGF- β 1 strongly correlates with its circulating amount, therefore positioning this secreted factor at the center of systemic homeostatic regulation.

Regulation of metabolism is one of the most vital control points for organismal health. Our study focused on caloric excess and high-fat diet as a model for how cardiac-derived TGF- β 1 can block adipocyte cell growth and confer protection against diet-induced weight gain, adiposity, inflammation, glucose intolerance, and liver triglyceride accumulation independent of food intake. Noteworthy, the role of TGF- β 1 in the prevention of triglyceride accumulation in the liver could also have translational implications for hepatic steatosis independent of the disease trigger. Altogether, these results are interesting and important, considering the above-mentioned complexity of TGF- β 1 signaling, as a clear understanding of its global metabolic effects is missing. Indeed, mouse models targeting, for example, canonical SMAD-dependent TGF- β 1 signaling specifically in adipocytes had suggested a positive impact of this factor in promoting adiposity [25]. This could be due to the fact that under physiological conditions, a balance of canonical and non-canonical intracellular pathways is operative in the determination of the final outcome of TGF- β 1 signaling. It is also important to consider that multiple growth factors utilize SMADs as intracellular signaling mediators, including growth and differentiation factors (GDFs) and bone morphogenic factors (BMPs), and, as such, elucidating the mechanisms underlying the phenotypes derived from SMAD genetic manipulation can be challenging. Another consideration to keep in mind is that while cell specific gene manipulation is critical to simplify complex systems and allow for easier data interpretation, *in vivo* all cell types within each tissue express receptors for TGF- β 1 and can therefore contribute to its overall final effects.

The observation that glucose tolerance is improved by cardiac-derived TGF- β 1 following 6 weeks of high-fat diet, when body mass and adiposity are reduced in TGF- β 1 mutant mice, but not when these parameters are unchanged between genotypes, suggests that alteration in glucose metabolism might not be a primary driver of the protective effects conferred by TGF- β 1. However, we did observe changes in white adipocyte metabolic gene expression and mitochondrial respiration prior to overt effects on body mass and adiposity. This is interesting as it suggests a role of TGF- β 1 in adipose tissue metabolism, which provides protection from adipocyte expansion and overall obesity under long-term exposure to high-fat diet. As protection from inflammation by TGF- β 1 was also evident already following 2 weeks of high-fat diet (the time point where TGF- β 1 mutant mice are indistinguishable from control animals in terms of body mass and adiposity), it is intriguing to speculate on a TGF- β 1-dependent connection between white adipocyte metabolism and inflammatory immune infiltration. In this regard, recent work has reported how enhancing the mitochondrial activity in white adipose tissue progenitor cells was effective in mitigating inflammation and protecting from diet-induced obesity [26]. Similarly, enhancement of oxidative

phosphorylation was shown to counteract pro-inflammatory activation of adipose tissue macrophages and improve obesity-associated metabolic dysfunction [27]. Noteworthy, while the regulation of cell metabolism was a clear common denominator of the mechanism of action of TGF- β 1 on white adipose tissue transcriptome, our results show the regulation of distinct transcripts by TGF- β 1 under control and high-fat diet. This is interesting as it highlights how stress modifies the transcriptional outcome of TGF- β 1 signaling. The indirect role of stress-induced co-factors for the orchestration of gene programs is, however, still undefined. Also, the respective contribution of direct TGF- β 1 signaling to white adipocyte versus systemic responses driven by organs other than white adipose tissue is still unclear.

In agreement with our model, the simultaneous overexpression of active TGF- β 1 from the liver, kidneys, and brown and white adipose tissue resulted in reduced body fat mass [28]. However, transgene expression in these animals was constitutive and not specifically induced in adulthood, which could have led to developmental defects underlying the observed multi-organ dysfunction. As such, the interpretation of the reported adipose tissue phenotype is complicated [28]. Nevertheless, the lipodystrophy reported in this study could suggest that, if chronic and uncontrolled, TGF- β 1 treatment could drive cachexia-like programs as seen in cancer [29]. It is interesting to note that another member of the TGF superfamily, TGF- β 2, was recently identified as an important mediator of the beneficial effects of exercise for systemic metabolic health. In the study by Goodyear and colleagues, exercise specifically induced TGF- β 2 in subcutaneous fat [30]. Therefore, it is possible that different tissues have evolved to utilize specific TGF mediators of systemic coordination to unique environmental challenges. It will be extremely interesting to understand in the future how individual TGF family members differentially operate during inter-organ communication. Our study sheds light on TGF- β 1 as a key mediator of heart-driven messages, and we cannot exclude the possibility that different organs might preferentially secrete different growth factors to deliver unique systemic messages.

Our study highlights cardiac-derived TGF- β 1 as a positive modulator of mitochondrial activity in white adipocytes. Although not addressed in this study, the increase in mitochondrial respiration in the white adipose tissue of TGF- β 1 mutant mice could be indicative of thermogenic potential, which could be an important topic for future research. Indeed, while mitochondrial content and activity are key differentiating features of brown adipose tissue, it is clear that white adipocytes are not metabolically inflexible as initially thought [31,32]. Indeed, a large body of evidence points to mechanisms that increase the mitochondrial activity of white adipose tissue as therapeutic value to counteract white adipocyte hypertrophy and consequent adiposity seen in obesity [33]. Considering the fundamental importance of TGF- β 1 for tissue homeostasis and injury responses, it is exciting to report a new role of this factor as a regulator of whole body metabolism.

4. METHODS

4.1. Animal generation and treatment

Male and female FVB/N mice up to 4 months of age were used in this study. The generation of cardiac-restricted TGF- β 1-overexpressing mice was achieved using an inducible double transgenic system as described previously [13]. Briefly, the alpha myosin heavy chain (α MHC) promoter is used to drive the expression of a transgene containing the tetracycline transactivator (tTA) coding sequence, specifically in cardiomyocytes. A second transgene, encoding for a constitutively active mutant form of TGF- β 1 (carrying a switch in cysteines 223 and 225 to serine to escape latency and guarantee

bioavailability) is also expressed within cardiomyocytes under the control of the α MHC promoter. This TGF- β 1 transgene is driven by a tetracycline response element (TRE), which is a nucleic acid sequence that contains multiple copies of the tetracycline operator sequence (tetO). The tetO sequences within the TRE are recognized and bound by the tTA protein, resulting in the activation of the TGF- β 1 transgene expression. In contrast, in the presence of doxycycline, the tTA protein is prevented from binding to the TRE, and the expression of the TGF- β 1 transgene is consequently inhibited. Breeding to generate our experimental mice was performed using doxycycline-containing food (625 mg/kg food; formulated by Purina) to ensure that the transgene remains off until weaning (4 weeks of age) and prevent any confounding effects of TGF- β 1 expression during pre- and post-natal development. tTA single transgenic mice served as control animals expressing WT levels of TGF- β 1. Control and experimental mice were littermates undergoing identical doxycycline treatment.

High-fat diet treatment was performed in 8- to 10-week-old TGF- β 1 gain-of-function mice and littermate controls for either 2 or 6 weeks (Research Diets Inc. D12492; 60% kcal fat, 20% kcal carbohydrate, 20% kcal protein, 5.21 kcal/g). Normal mouse chow (Envigo Teklad 7912; containing only 17% kcal fat and a total of 3.1 kcal/g) was used as control diet. For the measurement of food consumption under high-fat diet, mice of the same genotype were housed in couples and the food was weighted daily. These values for each cage were divided by two and normalized to body mass/day to measure the amount of food consumed by each mouse on average. The use of animals was approved by the Institutional Animal Care and Use Committee of The Ohio State University.

4.2. Energy balance and respiratory exchange ratio measurements

The mice were single housed 1 week prior to the experiment. After acclimation to single housing, the mice were placed in individual metabolic cages (Phenomaster, TSE Systems GmbH, Bad Homburg, Germany) for 7 days. Data on expired gases (VO_2 and VCO_2) and food and drink consumption were continuously collected. Individual mouse data from the last 5 days were averaged and used for the analysis. The respiratory exchange ratio (RER) was calculated as the VCO_2/VO_2 . Energy balance was obtained by calculating the difference between food intake (Kcal/h) and energy expenditure (Kcal/h). Energy expenditure was calculated using indirect calorimetry according to the equation $(3.941 * VO_2 + 1.106 * VCO_2)/1000$. ANCOVA was performed using body mass as the covariate.

4.3. Echocardiography and body composition measurements

Echocardiographic measurements were taken using a Vevo3100 Visual Sonics (Visual Sonics) system and MS-550 transducer as described previously [34]. The mice were lightly anesthetized (1.5% isoflurane) and echocardiographic parameters were determined in the M-mode using the parasternal short-axis view at the level of the papillary muscles. Measurements were calculated from the average of at least three consecutive cardiac cycles using the VevoLAB program.

An EchoMRI analyzer (EchoMRI LLC) was used to determine the body composition of mice. The device is first calibrated using a container of canola oil, as the NRM spectrum of this oil is comparable to that of the fat in mice. The mice are weighed and then placed in a plastic tube with a stopper that ensures that the mice stay as still as possible during measurement. The tube is then placed into the EchoMRI and the ~ 1 min measurement is initiated, outputting values for the total lean mass and total fat mass. The fat and lean mass percentages are calculated by dividing the total fat/lean mass by the total body mass.

4.4. Glucose tolerance and insulin sensitivity tests

A glucose tolerance test (GTT) was performed on mice fasted overnight (12 h) to minimize variability in baseline glucose values. Prior to the injection of glucose, the mice were weighed and placed on a tail injection platform, to minimize handling stress, and a 26G needle was used to penetrate the tail vein, and a drop of blood was withdrawn. A glucose strip (Unistrip1 generic blood glucose test) was inserted into the glucometer (OneTouch Ultra2, LifeScan) and the drop of blood was placed onto the tip of the strip to measure glucose. Glucose (Sigma—Aldrich) was prepared as a 20% v/v stock solution in PBS and sterile filtered. The volume of glucose to be injected was calculated based on weight to reach a target concentration of 2 g of glucose per 1 kg of weight. The mice were injected intraperitoneally and placed back into their cage until the next glucose measurement. Glucose was measured at 15, 30, 60, and 120 min following injection. Values for glucose were plotted against time to create a curve representing the response to glucose injection. GraphPad Prism software was used to calculate the area under the curve (AUC).

An insulin sensitivity test was performed as described for the GTT, but with the following changes. The mice were fasted for 2 h and injected with insulin, and glucose measurements were performed at 15, 30, 45, and 60 min following injection. A 0.1 U/mL working solution of insulin was prepared from a 100 U/mL stock (HumulinR—Lilly) in PBS and sterile filtered. The volume of insulin injected was based on weight, with a target concentration of 0.9 U of insulin per 1 kg of weight.

4.5. Flow cytometry

Adipose mononuclear cells were isolated from visceral white adipose tissue using a protocol adapted from one described previously for cardiac tissue [35]. Briefly, visceral white adipose tissue was collected immediately following euthanasia, washed with PBS, and weighed. A single-edged blade was used to mince tissue in a 10 cm cell culture plate and transferred to 50 mL conical tubes containing 3 mL of cold PBS. Following centrifugation at $100\times g$ for 2 min in a swinging-bucket rotor, the supernatant was decanted and 8 mL of collagenase II (1 mg/mL, DMEM) was added to each tube, followed by incubation at 37 °C for 20 min to facilitate tissue digestion. Tubes were mixed every 5 min during incubation. Digested tissue was filtered through a 40 μ m filter into fresh 50 mL conical tubes containing cold PBS supplemented with 0.5% (w/v) BSA and 2 mM EDTA. Any remaining chunks of tissue were triturated using the plunger of a 3 mL syringe. The filtrate was then centrifuged in a swinging-bucket rotor at $500\times g$ and 4 °C for 10 min, after which the supernatant was decanted. The pellet was then resuspended in 200 μ L of cold staining buffer, consisting of PBS supplemented with 0.5% (w/v) BSA and 1 mM EDTA, and fixed using 200 μ L of 1% paraformaldehyde. Complete fixation was ensured by incubating the tubes on ice for 10 min and any excess paraformaldehyde was neutralized using 1.8 mL of cold staining buffer. Post-fixation, these cells were pelleted using a swinging-bucket rotor at a speed of $500\times g$ for 10 min at 4 °C, after which the supernatant was decanted, and the cells were resuspended in 200–300 μ L of staining buffer. The resuspended cells were stored at 4 °C until staining (2–7 days).

All antibodies used (Invitrogen 25045182 — CD45 rat IgG2b kappa/PE-cyanine7; Invitrogen 63011280 — CD11b rat IgG2b kappa/Super Bright 600; Invitrogen 17003280 — CD3 rat IgG2b kappa/APC; Bio-Legend 123127 — F4/80 rat IgG2a kappa/PerCP cyanine5.5) were combined and added to each sample, followed by incubation on ice for 1 h. The isotype control antibodies used were Invitrogen 25403181 — rat IgG2b kappa/PE-cyanine7, Invitrogen 63403180 — rat IgG2b

kappa/Super Bright 600, Invitrogen 17403181 — rat IgG2b kappa/APC, and Invitrogen 45432180 — rat IgG2a kappa/PerCP cyanine5.5. To remove excess antibodies in solution, 4 mL of cold PBS was added to the cells, the cells were pelleted at 4 °C in a swinging-bucket rotor spinning at $500\times g$ for 10 min, the supernatant was decanted, and the pellets were reconstituted in 100–200 μ L of cold PBS. To accurately count cells, 2 μ L of Accucount beads (Spherotech ACBP-100-10) were added to each sample and the data were collected using a BD Fortessa flow cytometer, followed by analysis using FlowJo software. Following gating, events were normalized to both the internal control beads and initial tissue mass, with an output of normalized cells/mg of adipose tissue.

4.6. Triglyceride content measurements

Triglyceride content measurements were performed as described previously [36]. In brief, lipids were extracted from ~25 mg of tissue and triturated under liquid nitrogen using a Cole—Parmer Scientific tissue pulverizer, followed by immediate resuspension in 250 μ L ultrapure distilled water (Invitrogen). A 2:1 v/v chloroform:methanol solution was freshly prepared and 1 mL was added to each sample, followed by vortexing and incubation at RT for 5 min. The samples were centrifuged at $960\times g$ and RT for 5 min and the bottom layer of each sample was transferred to a fresh tube, rinsed with 50 mM NaCl, and centrifuged at $25,000\times g$ for 5 min at RT. The bottom layer was transferred to a fresh tube and rinsed with a 1:1 v/v CaCl₂ (0.36 M):methanol solution and centrifuged at $25,000\times g$ for 5 min. Lastly, the final bottom layer was transferred to a fresh tube and speed vacuumed before being reconstituted in 100% ethanol.

The triglyceride content was quantified using the Wako Diagnostics L-Type Triglyceride M kit (Cat. #'s 994-02891/990-02991), according to the manufacturer's instructions. Briefly, 4 μ L of each sample and water (blank), in addition to the prepared standards, were added to 90 μ L of reagent 1 in each well of a 96-well plate and mixed for 5 min at 37 °C. The absorbance of each well was then read at 600 nm and 700 nm. Next, 30 μ L of reagent 2 was added to each well, the plate was mixed for 5 min at 37 °C, and the absorbance of each well was measured at 600 nm and 700 nm. The final absorbances were calculated by subtracting the first measurements from the second; values for the standards were plotted against known concentration to create a standard curve that was used to determine the lipid abundance of the test samples.

4.7. Tissue staining and quantification

Tissues were fixed in 10% neutral buffered formalin for 18 h and processed for paraffin embedding. A Shandon Finesse 325 microtome (Thermo Scientific) was used to trim the surface of the paraffin blocks until all embedded tissues were exposed to air. The blocks were then placed face down in ice water overnight (heart, liver) or for 1 h (adipose) to hydrate the tissue. Once hydrated, the heart, liver, and brown adipose tissue blocks were cut in 5 μ m sections, whereas the white adipose tissue blocks were cut in 8 μ m sections. The paraffin sections were stained with hematoxylin & eosin (H&E), trichrome, or Picro-Sirius Red staining using standard procedures.

Images were taken using an EVOS Cell Imaging System (ThermoFisher) and quantifications were performed using ImageJ software. The total area of fibrosis on either the trichrome or Picro-Sirius-Red-stained images was measured using the threshold function within ImageJ, and this value is divided by the total area of tissue to calculate the percentage of fibrosis. Sections of adipose tissue stained with H&E were imaged and the adipocyte size was measured using ImageJ software. The scale was set by measuring the pixel length of the

scalebar and each adipocyte was individually traced using the free form tracing tool. The area inside of the tracing was measured and recorded. The calculation of lipid area in BAT was performed in ImageJ as follows: The tissue was traced and filled in with white, the image was converted to an 8-bit image, and the threshold function was used to measure the entire volume of the tissue. Adjustment of the threshold slider resulted in lipid droplets changing color and facilitated the measurement of the total lipid droplet volume. The percentage of the lipid droplet volume is derived by dividing the lipid droplet volume by the total tissue volume and multiplying this value by 100.

4.8. Western blotting and ELISA

Tissue protein extracts were generated using RIPA buffer (150 mM NaCl, 1% IGEPAL, 0.5% sodium deoxycholate, 0.1% SDS, 1 mM EDTA, 10 mM NaF, 50 mM Tris pH 7.4) with protease (cOmplete tablets, EDTA free, Roche) and phosphatase (phosphatase inhibitor cocktail sets I + II, Millipore) inhibitors. Standard Western blotting analysis was performed using 10% SDS-PAGE gels with the following primary antibodies from Cell Signaling: SMAD3 (1:1000, #9523), Phospho-SMAD3 (1:1000, #9520), SMAD2 (1:1000, #5339), Phospho-SMAD2 (1:1000, #3108), ERK1/2 (1:1000, #4695), Phospho-ERK1/2 (1:2000, #4370), p38 (1:1000, #8690), and Phospho-p38 (1:1000, #4511), and the following antibody from Abcam: Total OXPHOS Rodent WB Antibody Cocktail (1:5000, ab110413). Secondary antibody incubations were performed at room temperature for 60 min using HRP-conjugated antibodies (1:10,000) and then imaged using a ChemiDoc system (Bio-Rad).

Quantification of the TGF- β 1 content was performed on cardiac tissue and plasma using an ELISA kit by R&D Systems (DB100B) according to the manufacturer's instructions. The total TGF- β 1 amounts were measured by first activating the samples (to convert biologically inactive latent TGF- β 1 into active TGF- β 1) as instructed by the kit protocol, while measurement of the "bioavailable" TGF- β 1 content was performed by skipping the initial activation step.

4.9. mRNA analysis by real-time PCR

RNA was extracted using TRIzol (Ambion) and then reverse-transcribed using the High-Capacity cDNA Reverse Transcription kit (Applied Biosystems) as described previously [37]. Selected gene expression differences were analyzed by real-time quantitative PCR (qPCR) using SsoAdvanced SYBR Green Supermix (Bio-Rad) in a 96-well format and the ddCT method of analysis. Quantified mRNA levels were normalized to the housekeeping gene (*Ppia* in adipose tissue and *Rpl7* in heart), and expression is presented relative to control levels. The primers used were: mouse *CD74* 5'- GCTGGATGAAGCAGTGGCTCTT-3' and 5'- GATGTGGCT GACTTCTTCTGG-3'; mouse *Prdm165* 5'- GAACCAGGCATCCACTCGAA-3' and 5'- CGTGTCTCTGTGACTTCC-3'; mouse *Cpt2* 5'- GATGGCT-GAGTGCTCCAAATACC-3' and 5'- GCTGCCAGATACCGTAGAGCAA-3'; mouse *Hadha* 5'- GTTTGAGGACCTCGGTGTAAGC-3' and 5'- GAGAG-CAGATGTGTTGCTGGCA-3'; mouse *Glut4* 5'- TGGTTCAATGTGGCA-GAGCT-3' and 5'- AGATCTGGTCAAACGTCCGG-3'; mouse *Fabp4* 5'- TTTCTTCAAACCTGGGCGTG-3' and 5'- CACCAGCTTGTCACCATCTC-3'; mouse *Ppar α* 5'-CAAAGACGGGATGCTGATCG-3' and 5'-ATCCCCCTC TGCAACTTCTC-3'; mouse *Ppar γ* 5'- GAGGGCGATCTTGACAGGAA-3' and 5'- TGTGATCTCTTGACAGGCTT-3'; mouse *Ucp1* 5'- CGTCCCTG CCATTTACTGT-3' and 5'- ATGATGACGTTCCAGGACCC-3'; mouse Adiponectin 5'- AACTTGTGCGAGTTGGATGG-3' and 5'- GAGCGATACACA-TAAGCGGC-3'; mouse Leptin 5'- TTCTGTGGCTTTGGTCTTA-3' and 5'- AGCACATTTTGGGAAGGCAG-3'; mouse *Ppia* 5'-AGGTCTGGCATCTTGT

CC-3' and 5'-ATTCCTGGACCCAAAACGCT-3'; and mouse *Rpl7* 5'-TGGAACCATGGAGGCTGT-3' and 5'-CACAGCGGGAACCTTTTTC-3'.

4.10. Seahorse analysis

Mitochondria were isolated from the perigonadal WAT of WT and TGF mice and subjected to complementary electron coupling (EC) and electron flow (EF) assays using the Seahorse XFe96 Bioanalyzer, as described previously [2]. The EC assay measures the coupling between the electron transport chain (ETC) and oxidative phosphorylation, while EF assays determine the sequential flow of electrons through the different ETC complexes, independent of the proton gradient/membrane potential (i.e. in the uncoupled state). These assays utilize activators and inhibitors of ETC complexes I–V to fully investigate the mitochondrial function in real time.

4.11. RNA sequencing

RNA was extracted using a Zymo Research Quick-RNA MiniPrep kit (catalog no. R1055) and shipped for library preparation (DNBseq-G400 sequencing, transcriptome library, BGI Americas) and RNA sequencing (Complete Genomics, BGI Americas). Fastq files were checked for quality using FASTQC (<https://www.bioinformatics.babraham.ac.uk/projects/fastqc/>). Processed fastq files were aligned using Hisat2 [38] against the UCSC mm39 mouse genome (<https://hgdownload.soe.ucsc.edu/goldenPath/mm39/bigZips/>) and sorted using Samtools [39]. Sorted BAM files from Hisat2 were used as input for calculating forming count matrices using HTSeq [40]. GTF files matched to UCSC mm39 were used as the HTSeq index. HTSeq count matrices were combined and analyzed for differential expression using DESeq2 [41] with a Benjamini–Hochberg-adjusted p -value less than 0.05. All sequencing data are publically available through NIH Gene Expression Omnibus (Accession Number GSE179102). Heat maps were produced by using normalized read counts to calculate the Z-scores. Plotted transcripts are those significantly enriched in their respective categories by DESeq2. Gene ontology analysis was carried out on differentially expressed transcripts using the WEB-based gene set analysis toolkit (Webgestalt) [42]. Overrepresentation analysis was performed to analyze transcripts enriched in WT or TGF pgWAT under control or high fat diet. The background was set to protein coding transcripts. Categories were selected with an FDR value <0.05, with the minimum number of genes per category set to 10 and the maximum number of genes per category set to 2000.

4.12. Statistical analysis

All results were presented as mean \pm SEM, with dots indicating individual biological samples within a group. Statistical analysis between two groups was performed using the Student's 2-tailed t -test for normally distributed data with a p -value \leq 0.05 considered significant. For groups of 3, a 1-way ANOVA followed by Tukey's honestly significant difference (HSD) multiple-comparison test was performed, with statistical significance set at $\alpha = 0.05$. For groups of 2 genotypes and 2 conditions, a 2-way ANOVA followed by Tukey's HSD multiple-comparison test was performed, with statistical significance set at $\alpha = 0.05$. ANCOVA was performed to include body mass as the covariate in metabolic cage experiments. Bioinformatic statistics used default settings for each individual pipeline. In short, DESeq2 used a Benjamini–Hochberg-adjusted p -value. Data analysis was performed using GraphPad Prism 8 (GraphPad Software).

AUTHOR CONTRIBUTIONS

F.A. conceived the project. J.Z.L. performed most of the *in vivo* and *ex vivo* studies. J.M.P. performed triglyceride assays. C.R.M. performed flow cytometry. C.J.R. performed the initial high-fat-diet experiments. S.A.H. performed RNA sequencing analysis. L.E.D. performed echocardiography. J.S. and G.A.K. performed metabolic cage measurements. K.I.S. provided consultation on glucose test and high-fat-diet experimental design. K.K.B. and D.A.B. performed sea-horse analysis. J.Z.L. and F.A. wrote and revised the manuscript.

FUNDING

This work was supported by the NIH under grants [R01 HL 136951 and R01 HL 154001 to F.A.; R01 DK 127444 to G.A.K.; K01-DK116916 to K.K.B.; R01 HL138738 to K.I.S.] and by the US-Israel Binational Science Foundation (BSF) grant number 2017094 to F.A.

ACKNOWLEDGMENTS

We thank Heather Manning for technical assistance with the mitochondrial function studies.

CONFLICT OF INTEREST

None declared.

APPENDIX A. SUPPLEMENTARY DATA

Supplementary data to this article can be found online at <https://doi.org/10.1016/j.molmet.2021.101343>.

REFERENCES

- [1] Mitchell, N.S., Catenacci, V.A., Wyatt, H.R., Hill, J.O., 2011. Obesity: overview of an epidemic. *Psychiatric Clinics of North America* 34:717–732.
- [2] Baskin, K.K., Grueter, C.E., Kusminski, C.M., Holland, W.L., Bookout, A.L., Satapati, S., et al., 2014. MED13-dependent signaling from the heart confers leanness by enhancing metabolism in adipose tissue and liver. *EMBO Molecular Medicine* 6:1610–1621.
- [3] Priest, C., Tontonoz, P., 2019. Inter-organ cross-talk in metabolic syndrome. *Nature Metabolism* 1:1177–1188.
- [4] Kim, J.B., 2016. Dynamic cross talk between metabolic organs in obesity and metabolic diseases. *Experimental & Molecular Medicine* 48:e214.
- [5] de Bold, A.J., Flynn, T.G., 1983. Cardionatrin I - a novel heart peptide with potent diuretic and natriuretic properties. *Life Sciences* 33:297–302.
- [6] Sudoh, T., Kangawa, K., Minamino, N., Matsuo, H., 1988. A new natriuretic peptide in porcine brain. *Nature* 332:78–81.
- [7] Ferrero, K.M., Koch, W.J., 2020. Metabolic crosstalk between the heart and fat. *Korean Circulation Journal* 50:379–394.
- [8] Oreopoulos, A., Padwal, R., Kalantar-Zadeh, K., Fonarow, G.C., Norris, C.M., McAlister, F.A., 2008. Body mass index and mortality in heart failure: a meta-analysis. *American Heart Journal* 156:13–22.
- [9] Song, E.K., Lee, Y., Moser, D.K., Dekker, R.L., Kang, S.M., Lennie, T.A., 2014. The link of unintentional weight loss to cardiac event-free survival in patients with heart failure. *Journal of Cardiovascular Nursing* 29:439–447.
- [10] Khalil, N., 1999. TGF-beta: from latent to active. *Microbes and Infection* 1: 1255–1263.
- [11] Border, W.A., Noble, N.A., 1994. Transforming growth factor beta in tissue fibrosis. *New England Journal of Medicine* 331:1286–1292.
- [12] Grande, J.P., 1997. Role of transforming growth factor-beta in tissue injury and repair. *Proc Soc Exp Biol Med* 214:27–40.
- [13] Accornero, F., van Berlo, J.H., Correll, R.N., Elrod, J.W., Sargent, M.A., York, A., et al., 2015. Genetic analysis of connective tissue growth factor as an effector of transforming growth factor beta signaling and cardiac remodeling. *Molecular and Cellular Biology* 35:2154–2164.
- [14] Ackermann, M.A., Petrosino, J.M., Manring, H.R., Wright, P., Shettigar, V., Kilic, A., et al., 2017. TGF-beta1 affects cell-cell adhesion in the heart in an NCAM1-dependent mechanism. *Journal of Molecular and Cellular Cardiology* 112:49–57.
- [15] Litviňuková, M., Talavera-López, C., Maatz, H., Reichart, D., Worth, C.L., Lindberg, E.L., et al., 2020. Cells of the adult human heart. *Nature* 588:466–472.
- [16] Massague, J., Wotton, D., 2000. Transcriptional control by the TGF-beta/Smad signaling system. *The EMBO Journal* 19:1745–1754.
- [17] Suarez-Cuenca, J.A., De La Pena-Sosa, G., De La Vega-Moreno, K., Banderas-Lares, D.Z., Salamanca-García, M., Martínez-Hernández, J.E., et al., 2021. Enlarged adipocytes from subcutaneous vs. visceral adipose tissue differentially contribute to metabolic dysfunction and atherogenic risk of patients with obesity. *Scientific Reports* 11:1831.
- [18] Koenen, M., Hill, M.A., Cohen, P., Sowers, J.R., 2021. Obesity, adipose tissue and vascular dysfunction. *Circulation Research* 128:951–968.
- [19] Seale, P., Bjork, B., Yang, W., Kajimura, S., Chin, S., Kang, S., et al., 2008. PRDM16 controls a brown fat/skeletal muscle switch. *Nature* 454:961–967.
- [20] Seale, P., Kajimura, S., Yang, W., Chin, S., Rohas, L.M., Uldry, M., et al., 2007. Transcriptional control of brown fat determination by PRDM16. *Cell Metabolism* 6:38–54.
- [21] Lim, H., Zhu, Y.Z., 2006. Role of transforming growth factor-beta in the progression of heart failure. *Cellular and Molecular Life Sciences* 63:2584–2596.
- [22] Koli, K., Myllarniemi, M., Keski-Oja, J., Kinnula, V.L., 2008. Transforming growth factor-beta activation in the lung: focus on fibrosis and reactive oxygen species. *Antioxidants and Redox Signaling* 10:333–342.
- [23] Alves, M.J., Figueredo, R.G., Azevedo, F.F., Cavallaro, D.A., Neto, N.I.P., Lima, J.D.C., et al., 2017. Adipose tissue fibrosis in human cancer cachexia: the role of TGFbeta pathway. *BMC Cancer* 17:190.
- [24] Greco, S.H., Tomkotter, L., Vahle, A.K., Rokosh, R., Avanzi, A., Mahmood, S.K., et al., 2015. TGF-beta blockade reduces mortality and metabolic changes in a validated murine model of pancreatic cancer cachexia. *PLoS One* 10: e0132786.
- [25] Yadav, H., Quijano, C., Kamaraju, A.K., Gavrilo, O., Malek, R., Chen, W., et al., 2011. Protection from obesity and diabetes by blockade of TGF-beta/Smad3 signaling. *Cell Metabolism* 14:67–79.
- [26] Joffin, N., Paschoal, V.A., Gliński, C.M., Crewe, C., Elnwasany, A., Szewda, L.I., et al., 2021. Mitochondrial metabolism is a key regulator of the fibro-inflammatory and adipogenic stromal subpopulations in white adipose tissue. *Cell Stem Cell* 28:702–717 e708.
- [27] Wang, Y., Tang, B., Long, L., Luo, P., Xiang, W., Li, X., et al., 2021. Improvement of obesity-associated disorders by a small-molecule drug targeting mitochondria of adipose tissue macrophages. *Nature Communications* 12:102.
- [28] Clouthier, D.E., Comerford, S.A., Hammer, R.E., 1997. Hepatic fibrosis, glomerulosclerosis, and a lipodystrophy-like syndrome in PEPCk-TGF-beta1 transgenic mice. *Journal of Clinical Investigation* 100:2697–2713.
- [29] Guttridge, D.C., 2015. A TGF-beta pathway associated with cancer cachexia. *Nature Medicine* 21:1248–1249.

- [30] Takahashi, H., Alves, C.R.R., Stanford, K.I., Middelbeek, R.J.W., Nigro, P., Ryan, R.E., et al., 2019. TGF-beta2 is an exercise-induced adipokine that regulates glucose and fatty acid metabolism. *Nature Metabolism* 1:291–303.
- [31] Young, P., Arch, J.R., Ashwell, M., 1984. Brown adipose tissue in the parametrial fat pad of the mouse. *FEBS Letters* 167:10–14.
- [32] Vitali, A., Murano, I., Zingaretti, M.C., Frontini, A., Ricquier, D., Cinti, S., 2012. The adipose organ of obesity-prone C57BL/6J mice is composed of mixed white and brown adipocytes. *The Journal of Lipid Research* 53:619–629.
- [33] Lee, J.H., Park, A., Oh, K.J., Lee, S.C., Kim, W.K., Bae, K.H., 2019. The role of adipose tissue mitochondria: regulation of mitochondrial function for the treatment of metabolic diseases. *International Journal of Molecular Sciences* 20.
- [34] Dorn, L.E., Lawrence, W., Petrosino, J.M., Xu, X., Hund, T.J., Whitson, B.A., et al., 2021. Microfibrillar-associated protein 4 regulates stress-induced cardiac remodeling. *Circulation Research* 128:723–737.
- [35] Covarrubias, R., Ismahil, M.A., Rokosh, G., Hamid, T., Accornero, F., Singh, H., et al., 2019. Optimized protocols for isolation, fixation, and flow cytometric characterization of leukocytes in ischemic hearts. *American Journal of Physiology - Heart and Circulatory Physiology* 317:H658–H666.
- [36] Petrosino, J.M., Longenecker, J.Z., Ramkumar, S., Xu, X., Dorn, L.E., Bratasz, A., et al., 2021. Paracardial fat remodeling affects systemic metabolism through alcohol dehydrogenase 1. *Journal of Clinical Investigation*, 131.
- [37] Accornero, F., Schips, T.G., Petrosino, J.M., Gu, S.Q., Kanisicak, O., van Berlo, J.H., et al., 2017. BEX1 is an RNA-dependent mediator of cardiomyopathy. *Nature Communications* 8:1875.
- [38] Kim, D., Paggi, J.M., Park, C., Bennett, C., Salzberg, S.L., 2019. Graph-based genome alignment and genotyping with HISAT2 and HISAT-genotype. *Nature Biotechnology* 37:907–915.
- [39] Li, H., Handsaker, B., Wysoker, A., Fennell, T., Ruan, J., Homer, N., et al., 2009. The sequence alignment/map format and SAMtools. *Bioinformatics* 25:2078–2079.
- [40] Anders, S., Pyl, P.T., Huber, W., 2015. HTSeq—a Python framework to work with high-throughput sequencing data. *Bioinformatics* 31:166–169.
- [41] Love, M.I., Huber, W., Anders, S., 2014. Moderated estimation of fold change and dispersion for RNA-seq data with DESeq2. *Genome Biology* 15:550.
- [42] Liao, Y., Wang, J., Jaehnig, E.J., Shi, Z., Zhang, B., 2019. WebGestalt 2019: gene set analysis toolkit with revamped UIs and APIs. *Nucleic Acids Research* 47:W199–W205.